pp 1239–1260. © Royal Aeronautical Society 2017
doi: 10.1017/aer.2017.55

Numerical simulation of circulation control turbine cascade with Coanda jet and counter-flow blowing at high Mach numbers

Y. Feng
fengyanyanhit@gmail.com

Y. Song and F. Chen
School of Energy Science and Engineering
Harbin Institute of Technology
Harbin
China

ABSTRACT

The performance of a circulation-control inlet guide vane that makes use of the Coanda effect was studied numerically in a high Mach number turbine cascade. The effect of different shapes (elliptic and circular) of the Coanda surface at the blade trailing edge was investigated by implementing both a Coanda jet and a counter-flow blowing. Under high subsonic flow conditions, with a total blowing ratio of 3% of the mainstream, the circulation control cascade can reach the same performance as the reference stator with a 13.5% reduction in the axial chord length, with minimal increase of the energy loss coefficient. The Coanda surfaces with small curvature are more efficient in entraining the mainstream flow, and they achieve better aerodynamic performance. The wall attachment of the Coanda jet is improved by employing counter-flow blowing, resulting in a slight increase of both the exit flow angle and the expansion ratio. Under supersonic flow conditions at the cascade exit, it is more difficult for the circulation control cascade to reach the appropriate flow turning due to a premature shock wave, which is absent in the original cascade until the very end of the suction surface.

Keywords: Coanda effect; gas turbine cascade; circulation control; Mach number; Coanda jet; counter-flow blowing

Received 10 September 2016; revised 4 May 2017; accepted 15 May 2017; first published online 19 June 2017.

NOMENCLATURE

L	chord length, m
$\dot{m}$	mass flow rate, kg/s
n	sequence number of circular/elliptic Coanda surface
t	pitch, m
y^+	dimensionless wall distance
C	Circular
CC	Circulation Control
CFB	Counter-Flow Blowing
CJ	Coanda Jet
C_f	friction coefficient, $C_f = \frac{\tau_\omega}{P_e^* - P_e}$
C_p	pressure coefficient, $C_p = \frac{P - P_e}{P_e^* - P_e}$
C_μ	momentum coefficient
E	Elliptic
Ma	Mach number
IGV	Inlet Guide Vane
L.E.	Leading Edge
P.S.	Pressure Side
P	static pressure, Pa; or pressure side curve
Re	Reynolds number
S	dimensionless arc length of Coanda surface
S'	dimensionless arc length of pressure surface or suction surface
S.S.	Suction Side
T.E.	Trailing Edge
V	velocity, m/s
α	exit flow angle, degree
γ	specific-heat ratio
λ	stagger angle, degree
π	expansion ratio
τ_ω	wall shear stress, kg/(m×s^2)
ζ	energy loss coefficient

Subscripts

0	cascade without blowing
ax	axial
e	cascade exit conditions
i	cascade inlet conditions
$j1$	inlet conditions of Coanda jet
$j2$	inlet conditions of counter-flow blowing
∞	main flow conditions

Superscript

$*$	total conditions

https://doi.org/10.1017/aer.2017.55 Published online by Cambridge University Press

1.0 INTRODUCTION

A near-wall jet around a curved surface is subject to centrifugal acceleration and the associated radial pressure gradient. Under the balance of these two forces, the jet will remain attached to the curved wall. This phenomenon is known as the Coanda effect or wall attachment effect. The jet can achieve a high entrainment, and the Coanda effect concept has been used as a circulation control (CC) method on aerofoils since the 1960s. Englar[1] provided a broad overview of the application of CC technology, such as lift augmentation, drag decrease/increase, stability enhancement, pitching, pneumatic propulsion, etc.. Kweder et al.[2] reviewed the detailed development process of CC technology over the past 60 years. During an investigation of circulation controlled flaps, Jones et al.[3] pointed out that as the area of the Coanda surface increases, the Coanda effect generates more lift, but the drag increases as well due to the blunt trailing edge. Cook et al.[4] tested a prototype of a circulation control actuator in a flapless flight and found that suitable blowing can neutralise the drag produced by the blunt trailing edge. Liu and Sankar[5] performed a numerical study about applying tangential blowing on the edge of a wing. The results showed that it has the potential of controlling the tip vortex and reducing the blade/vortex interaction noise. In order to find the structure providing the largest lift augmentation, Kanistras et al.[6] tested three circulation control wings (S8036 aerofoil, NACA0015 aerofoil, and NACA2412 aerofoil) in a low-speed wind tunnel. The circulation control aerofoils are also proved to be efficient under high-speed conditions[7,8]. Through both computational fluid dynamics (CFD) and wind tunnel testing, the Air Force Research Laboratory (AFRL) used a circulation control wing (CCW) to develop 'speed agility,' a phrase coined for an aircraft that is capable of efficient flight at low speeds and at transonic cruise speeds, in its SACD (Speed Agile Concept Demonstrator) program[9-12]. NASA has carried out CFD studies and wind tunnel experiments on the CC technology. Jones et al.[13] developed a systematic approach of wind tunnel experiments to generate benchmark quality experimental data. Milholen et al.[14] and Chan et al.[15] conducted some wind tunnel tests of the FAST-MAC (Fundamental Aerodynamics Subsonic/Transonic-Modular Active Control) circulation control model under transonic and high Reynolds number conditions.

Forster and Steijl[16] did detailed CFD studies, including grid requirements and turbulence models, of circulation control at up to freestream $Ma = 0.8$. Forster et al.[17] performed a multipoint optimisation study for the Coanda surface of a supercritical aerofoil. The resulting multipoint-designed shape performed favourably at high blowing ratios. Diskin et al.[18] conducted a detailed grid convergence study by using three CFD codes on two-dimensional (2D) turbulent flows around the NACA 0012 aerofoil and a flat-plate configuration. The solutions computed by different codes on different grid families appeared to converge to the same continuous limit but exhibited strikingly different convergence characteristics.

After its successful application in the external flow around an aerofoil, the CC technology was applied to internal flows. In an axial compressor inlet guide vane (IGV), Kruger et al.[19] obtained a maximum flow deflection of 13.5° by using blown flaps with a mechanical flap angle of 45°. In 2000, when introducing flow control technologies in gas turbine, Lord et al.[20] pointed out that the Coanda jet could be used to replace complicated mechanical devices for transforming the yaw angle at the rotor inlet of the fan and to achieve the goals of weight saving, cost reduction, and a simpler fan system. To reach a design turning angle of 11° in a compressor, Hill et al.[21] optimised several parameters of a circulation control IGV, including jet height, radius of the Coanda surface, and the air supply pressure. The optimal case obtained the designed flow-turning angle with half the number of blades, which indicated that a circulation control IGV might provide an alternative to current flap IGV. In the design

https://doi.org/10.1017/aer.2017.55 Published online by Cambridge University Press

Table 1
Geometric parameters of the stator cascade

Aspect ratio	Solidity	Camber angle	Stagger angle
1.67	1.1	73.5°	33.25°

of a CC stator with blowing air close to the trailing edge, Guendogdu et al.[22] and Fischer et al.[23,24] found that the modified stator with a decrease in the cascade solidity could achieve the same or even larger turning angles than the reference stator. With the object of increasing the circulation around the blade and achieving considerable flow vectoring, Harff et al.[25] applied both Coanda jet and counter-flow blowing (CFB) in circulation control IGVs. The results showed that the CFB further improved the flow-turning angle compared to the Coanda jet alone, but increased the loss coefficient.

Song et al.[26] first applied the Coanda effect to a gas turbine blade at an exit Mach number of 0.3. The main advantages of the CC turbine cascade were simplification of the cooling structure and reduction of the blade weight. The results showed that, with a tolerable jet pressure consumption, the performance of a CC turbine cascade was capable of achieving or exceeding that of the original cascade, which indicated the promising potential of the circulation control technology in turbine cascades. As current gas turbines usually work at high subsonic and supersonic flow conditions, the mechanism and performance of the Coanda effect applied to high-speed internal flows could also be valuable.

This paper presents a continuation of the investigation of Ref. 26 in a CC turbine cascade at transonic Mach numbers 0.60, 0.85, and 1.10. The research objective was to reduce the axial length of the turbine stator while maintaining the designed turning angle and expansion ratio, and low aerodynamic losses. The performance of the elliptic and circular Coanda surfaces was investigated and compared with the original cascade. The counter-flow blowing on the pressure side was also studied to investigate its capability of improving the jet attachment and entrainment of the mainstream flow.

2.0 GEOMETRY OF THE ORIGINAL AND CIRCULATION CONTROL CASCADES

Table 1 provides the main geometric parameters of the original stator cascade (the baseline). The circulation control cascade was constructed by modifying the blade trailing edge of the baseline.

The configurations of the original stator blade, the Coanda surfaces, and the jet slots are shown in Fig. 1. The Coanda jet (CJ) injects from a nozzle slot with a height of 0.5 mm on the suction surface (point A), which is located at 85% axial chord length (l_{ax}) downstream of the leading edge. In Fig. 1(b), the vertical line AB reaches point 1 on the pressure surface; line AC is perpendicular to the suction surface at point A and reaches point 4 on the pressure surface. Points 2 and 3 are the quarter point and midpoint of the curve 14 on pressure surface. The Coanda surfaces start immediately aft of the Coanda jet and end at three different ending points (1, 2 and 3) on the pressure surface. The beginning parts of the Coanda surfaces are tangent to the local suction surface (thus the Coanda jet injects into the cascade channel tangentially to the local flow). Between the start point and each ending point, circular and elliptic Coanda surfaces were designed. Sequence numbers according to the ending points

https://doi.org/10.1017/aer.2017.55 Published online by Cambridge University Press

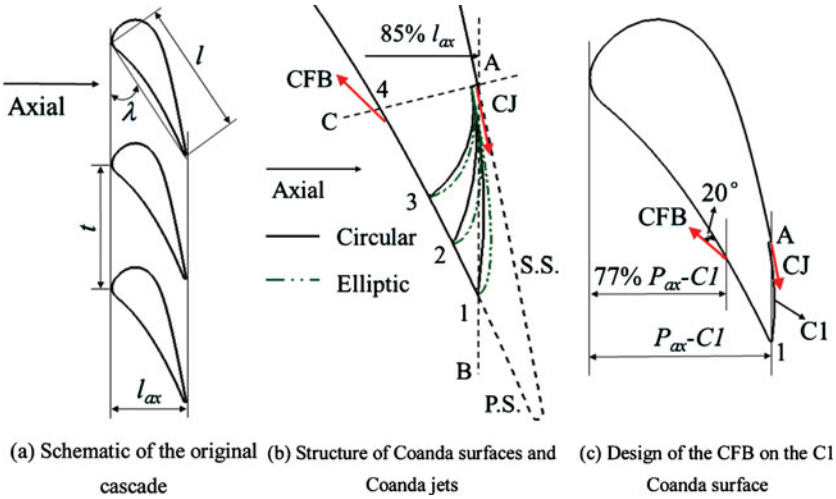

(a) Schematic of the original cascade (b) Structure of Coanda surfaces and Coanda jets (c) Design of the CFB on the C1 Coanda surface

Figure 1. (Colour online) Sketches of the cascade geometry, Coanda surfaces, and jet slots.

were given, i.e., C1, C2 and C3 for circular Coanda surfaces, and E1, E2 and E3 for elliptic ones. From C1 to C3, the radius of the Coanda surface becomes smaller while the curvature increases; the curvature along the elliptic Coanda surface varies, but at the front part of Coanda surface, the curvature becomes larger from E1 to E3. Moreover, by using Coanda surfaces to replace the original trailing edge, the axial length of the blade is shortened. For the CC cascade with circular Coanda surfaces, the values of axial chord length are 86.48% (C1), 84.80% (C2), and 84.10% (C3) of the baseline. For the CC cascade with elliptic Coanda surfaces, the values are 88.07% (E1), 85.64% (E2), and 84.31% (E3) of the baseline.

By pushing back the position of the front and rear stagnation point, the circulation around the aerofoil was increased. In order to achieve high lift around the circulation control blade, counter-flow blowing on the pressure side was added in the CC cascade with circular Coanda surfaces. The locations of the CFB were designed for each circular Coanda surface individually. Taking the C1 Coanda surface for an example, as shown in Fig. 1(c), the axial length of the revised pressure surface of the CC blade is denoted by P_{ax}-*C1* and, correspondingly, P_{ax}-*C2* for the C2 Coanda surface and P_{ax}-*C3* for the C3 Coanda surface. The CFB slot is located at 77% P_{ax}-*C1* (same ratio for C2 and C3) downstream of the leading edge of the pressure surface. The CFB injects upstream into the flow at an angle of 20° relative to the local tangential direction.

3.0 NUMERICAL METHOD AND CFD VALIDATION

The commercial software ANSYS CFX[27] was used to perform the 2D steady numerical simulations. The k-ω SST (shear stress transport) turbulence model was chosen. Due to the periodicity of the flow passage, a single flow passage was used as the computational domain to reduce the calculation effort. The 2D structured mesh shown in Fig. 2 was generated by ANSYS ICEM[28]. There were approximately 40,000 cells in the computational domain. For the circulation control cascades, the topology of the mesh was similar to the baseline. The grid requirement near rigid walls of the k-ω SST turbulence model is satisfied by a boundary-layer refinement leading to a y^+value smaller than 1. Figure 2(b) shows an enlarged view of the grid

https://doi.org/10.1017/aer.2017.55 Published online by Cambridge University Press

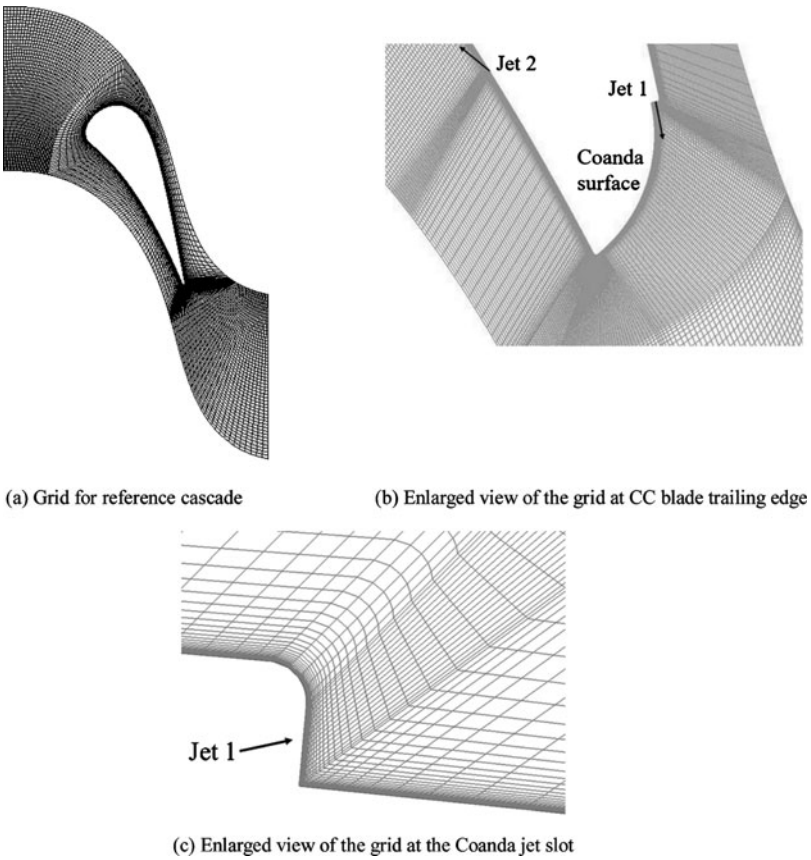

(a) Grid for reference cascade

(b) Enlarged view of the grid at CC blade trailing edge

(c) Enlarged view of the grid at the Coanda jet slot

Figure 2. Grid for the turbine cascade without and with the jet slots.

around the trailing edge of the CC cascade and Fig. 2(c) grid at the Coanda jet slot. To capture the flow details accurately, the density of the grid at the jet inlets was increased compared to the adjacent region. As a result, the total number of grid increases to about 46,000 for the circulation control cascades.

The numerical simulations on the baseline cascade and the circulation control cascades were conducted with boundary conditions as follows. The blade surface was no slip, smooth, and adiabatic. A translational periodicity condition was chosen for the two sides of the computational domain. The cascade inlet is located at 80% of the axial chord length before the cascade leading edge and the cascade outlet is 80% of the axial chord length after the cascade trailing edge. At the cascade inlet, an axial inflow was given (namely, the angle-of-attack is 0°) with a constant total temperature (380 K) and turbulence intensity (5%). Total pressure at the inlet and static pressure at the outlet were selected in order to obtain the specified exit Mach numbers (0.60, 0.85 and 1.10). Even though high jet momentum or high jet velocity will increase the effect of the circulation control actuator, the total pressure at the two jet inlets was given to be exactly the same as the total pressure at the cascade inlet for each exit Mach number condition in this study. Thus, the supply pressure ratio (defined as the ratio of jet total pressure to cascade inlet total pressure) was 1.0. Hence, no additional devices will be needed in practice to provide pressurised gas. The jet develops naturally out of the slot, and

https://doi.org/10.1017/aer.2017.55 Published online by Cambridge University Press

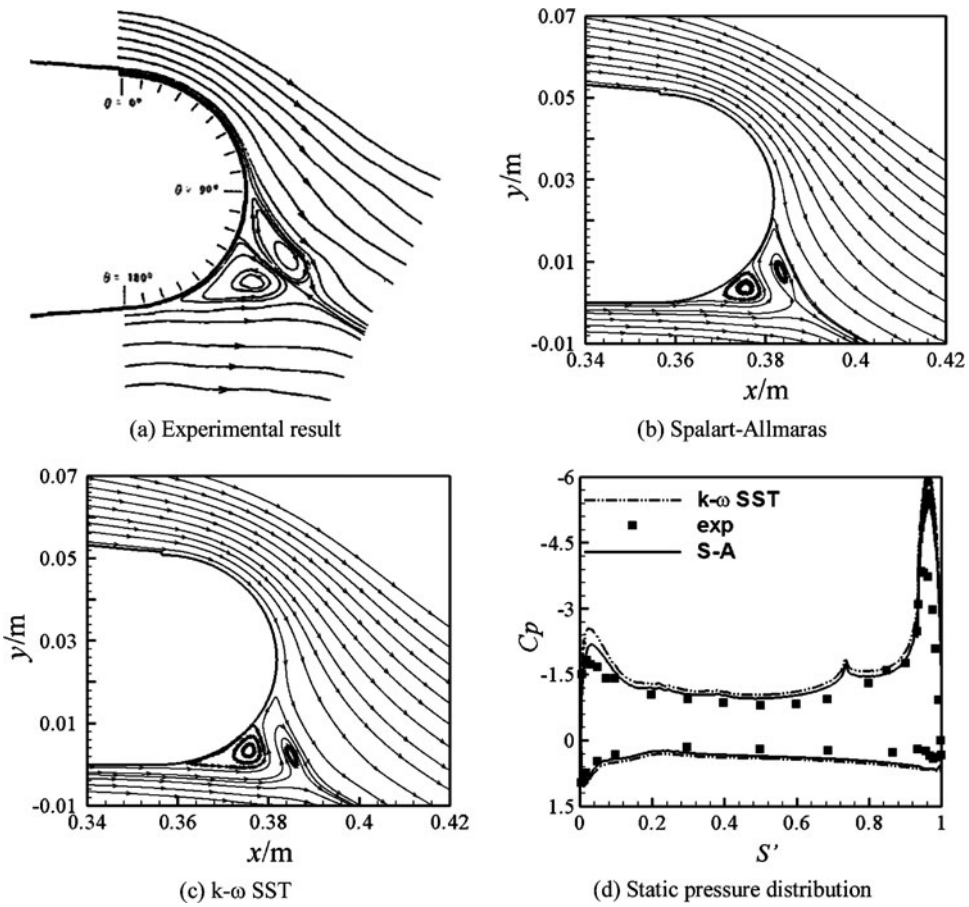

Figure 3. Comparison of streamlines near the aerofoil trailing edge and static pressure distribution along the aerofoil, $V_\infty = 42.5\,\mathrm{m/s}$, $C_\mu = 0.031$, $Re = 1\times10^6$ (based on aerofoil chord length).

the jet velocity profile is probably not uniform. For each CC cascade case, the jet mass flow was less than 4% of the mainstream flow, and the jet velocity was slightly higher than that at the exit of the cascade.

To test the accuracy of the numerical method, a simulation of a circulation control wing of the Lockheed Georgia (CCW-LG)[29] was performed first. The numerical results were compared to the existing experimental results obtained by Lockheed Georgia in 1986. The velocity of the oncoming flow is 42.5 m/s and the Reynolds number based on the aerofoil chord length is 1×10^6 in their experiments. The geometry of the aerofoil profile and jet orifice can be found in Ref. 29. Several turbulence models, including Spalart-Allmaras, k-ε Standard, k-ε Realizable, k-ω Standard, k-ω SST and Reynolds stress-QPS, etc. were tested with a jet velocity ratio of 3.44 (or a jet momentum coefficient C_μ of 0.031).

Figure 3 shows the comparison of the streamlines at the aerofoil trailing edge and the static pressure distribution along the aerofoil between the experimental[29] and the numerical results. The results from Fig. 3(a) to Fig. 3(c) show that the two vortices at the trailing

https://doi.org/10.1017/aer.2017.55 Published online by Cambridge University Press

edge are predicted accurately via Spalart-Allmaras and k-ω SST turbulence models. Other turbulence models failed to predict the flow condition at the trailing edge precisely, and the results are not shown here. The numerical results of the static pressure distribution shown in Fig. 3(d) are consistent with the experiment data. Except at the end of the Coanda surface, the numerical pressure is slightly lower than the experimental results. The above observation suggests that the numerical results obtained by Spalart-Allmaras and k-ω SST turbulence models are more reliable than those predicted by other turbulence models for this geometry. In the following numerical study on the circulation-control turbine cascade, the k-ω SST turbulence model was applied.

The simulation using different grid density was conducted and the distribution of Mach number around the blade profile was compared at three outlet flow conditions, i.e., 0.60, 0.85 and 1.1. When the outflow is a high subsonic condition, the numerical results are generally consistent with the experimental observations. When the outflow is supersonic condition, the numerical results have some deviation compared with the experimental results. But the trend of the Mach number around the blade is the same. The position and strength of the shock wave are reflected relatively accurately by CFD method. Therefore, the accuracy level of the CFD results is acceptable to a certain extent. However, for some reason, the experimental results are not provided here.

Three parameters were considered to evaluate the aerodynamic performance of the circulation control cascade. They are the exit flow angle, expansion ratio, and energy loss coefficient at the cascade outlet, which is at 80% axial chord length after the trailing edge of the blade. The exit flow angle α is the pitch-averaged flow angle at the cascade outlet in respect to the axis. The expansion ratio π is the ratio of the static pressure at cascade inlet to that at cascade outlet. For the original cascade, the energy loss coefficient ζ_0 is calculated by Equation (1). For the circulation control cascade, the corrected energy loss coefficient ζ is calculated by Equation (2), in which $\overline{P^*}$ is a modified inlet total pressure to account for the power consumption of the jets. The definition of $\overline{P^*}$ is shown in Equation (3). For the cases without counter-flow blowing, $\dot{m}_{j2}$ and P^*_{j2} equal 0 in Equation (3).

$$\zeta_0 = \frac{\left(P_e/P_e^*\right)^{\frac{\gamma-1}{\gamma}} - \left(P_e/P_i^*\right)^{\frac{\gamma-1}{\gamma}}}{1 - \left(P_e/P_i^*\right)^{\frac{\gamma-1}{\gamma}}} \quad \ldots (1)$$

$$\zeta = \frac{\left(P_e/P_e^*\right)^{\frac{\gamma-1}{\gamma}} - \left(P_e/\overline{P^*}\right)^{\frac{\gamma-1}{\gamma}}}{1 - \left(P_e/\overline{P^*}\right)^{\frac{\gamma-1}{\gamma}}} \quad \ldots (2)$$

$$\overline{P^*} = \frac{\dot{m}_i P_i^* + \dot{m}_{j1} P_{j1}^* + \dot{m}_{j2} P_{j2}^*}{\dot{m}_i + \dot{m}_{j1} + \dot{m}_{j2}} \quad \ldots (3)$$

4.0 RESULTS AND DISCUSSION

4.1 Results at *Ma* = 0.60

Figure 4 shows the aerodynamic performance of the turbine cascade for exit Mach number of 0.60, in which the values of 1, 2 and 3 on the abscissa represent the sequence numbers of the circulation control cascade with circular (C1 to C3) and elliptic (E1 to E3) Coanda surfaces. The labels 'elliptic_1 jet' and 'circular_1 jet' denote the cases with only the Coanda jet applied. Correspondingly, the label 'circular_2 jets' represents the circular Coanda surfaces

https://doi.org/10.1017/aer.2017.55 Published online by Cambridge University Press

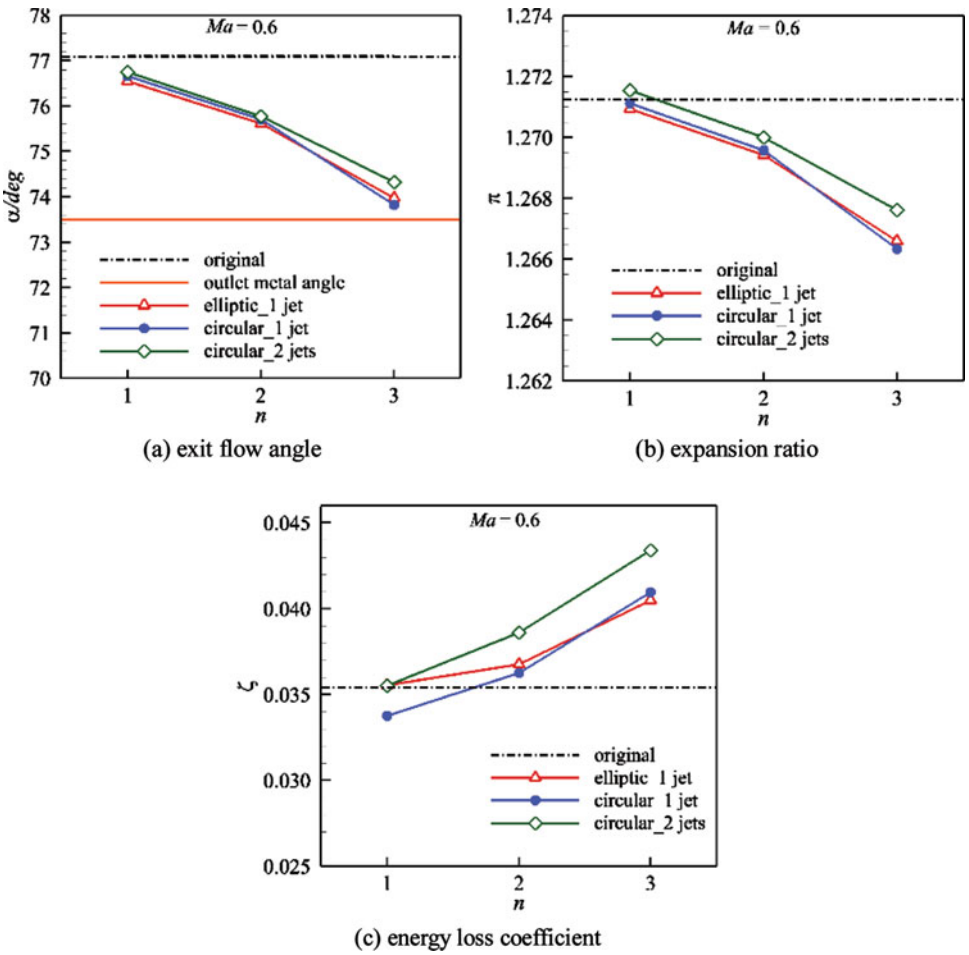

Figure 4. (Colour online) Performance parameters of the cascades, $Ma = 0.60$.

with both the Coanda jet and the counter-flow blowing. Code names are given to different cases mentioned in the following. For example, case 'C3_1 jet' indicates the circulation control cascade that has the circular Coanda surface with the largest curvature at the trailing edge and with the Coanda jet alone. In each plot, the horizontal dashed line indicates the parameter value of the original cascade as the baseline. The horizontal solid line in Fig. 4(a) represents the outlet metal angle (73.5°) of the original blade. In general, the elliptic and circular Coanda surfaces with the same end points have similar performance. That is because the initial curvature values of the elliptic and circular surfaces are close. The trend of the expansion ratio is similar to that of the exit flow angle. The increasing curvature of the Coanda surface leads to early detachment of the Coanda jet. The aerodynamic performance of the circulation control cascades decreases with the increasing of the curvature of Coanda surface (or curvature at the front part of elliptic surfaces), resulting in the reduction of the exit flow angle and expansion ratio, as well as the augmentation of the energy loss coefficient. With the counter-flow blowing on the pressure side, the flow-turning angle and the expansion ratio

https://doi.org/10.1017/aer.2017.55 Published online by Cambridge University Press

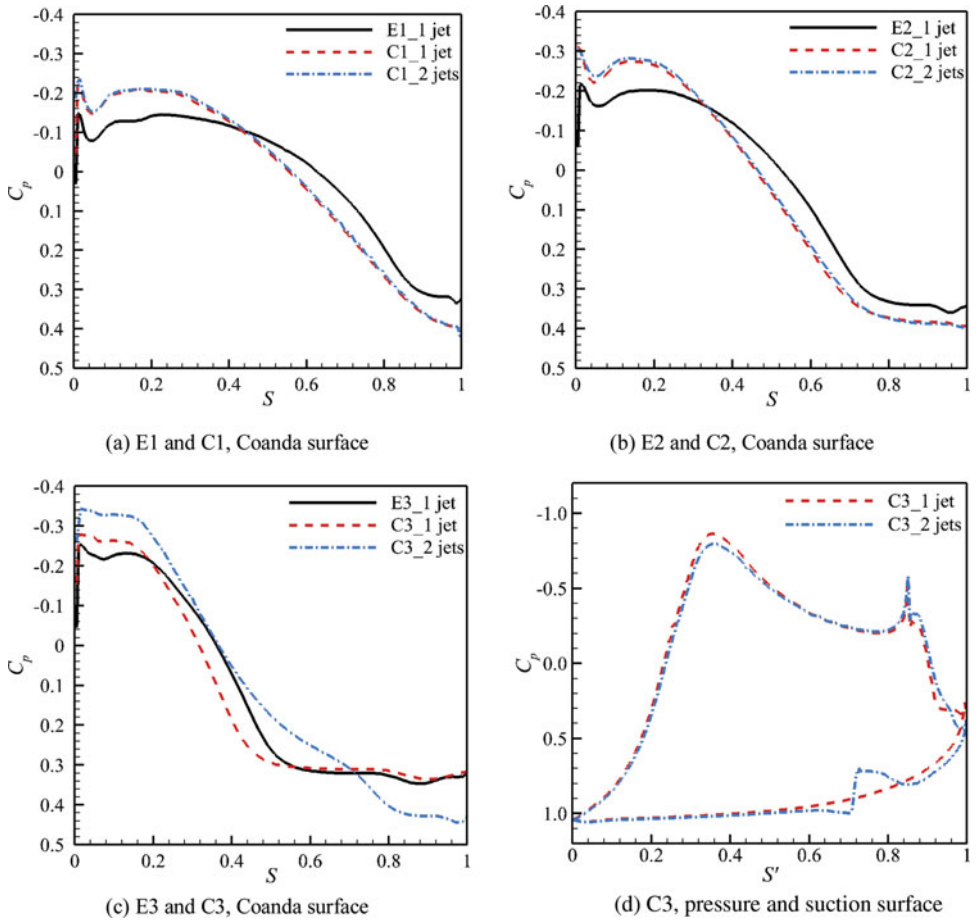

Figure 5. (Colour online) Distribution of wall pressure coefficient on the Coanda surfaces, $Ma = 0.60$.

go up slightly for all the circulation control cascades. As the consumption of the jet supply pressure increases, the loss coefficients increase compared to the Coanda jet alone.

From Fig. 4, the circulation control cascades with E1 and C1 Coanda surfaces achieve the flow turning angle and expansion ratio of the baseline with similar or smaller energy loss coefficient. At the same time, the jet mass flow rate is about 3% of the main flow, and the axial chord lengths are shortened by 11.9% for E1 and 13.5% for C1 compared with the original cascade. The results indicate that the benefit of the CC technology counteracts the disadvantages of the extra energy expenditure by the jets and the shortened flow passage. Although the CC cascades achieve slightly less flow turning than the baseline, they still meet the incidence requirement of the downstream cascade with the exit flow angle above 73.5°. The expansion ratio decreases slightly with increasing the curvature of the Coanda surface. The worst result comes from case C3_1 jet, but its expansion ratio is still 99.6% of the baseline. Case C3 has the shortest axial chord length, with a large separation region near the trailing edge, as shown in Fig. 7. With extra energy consumption from both the Coanda jet and CFB, case C3_2 jets havethe highest energy loss coefficient, which is 22.6% higher than the baseline.

https://doi.org/10.1017/aer.2017.55 Published online by Cambridge University Press

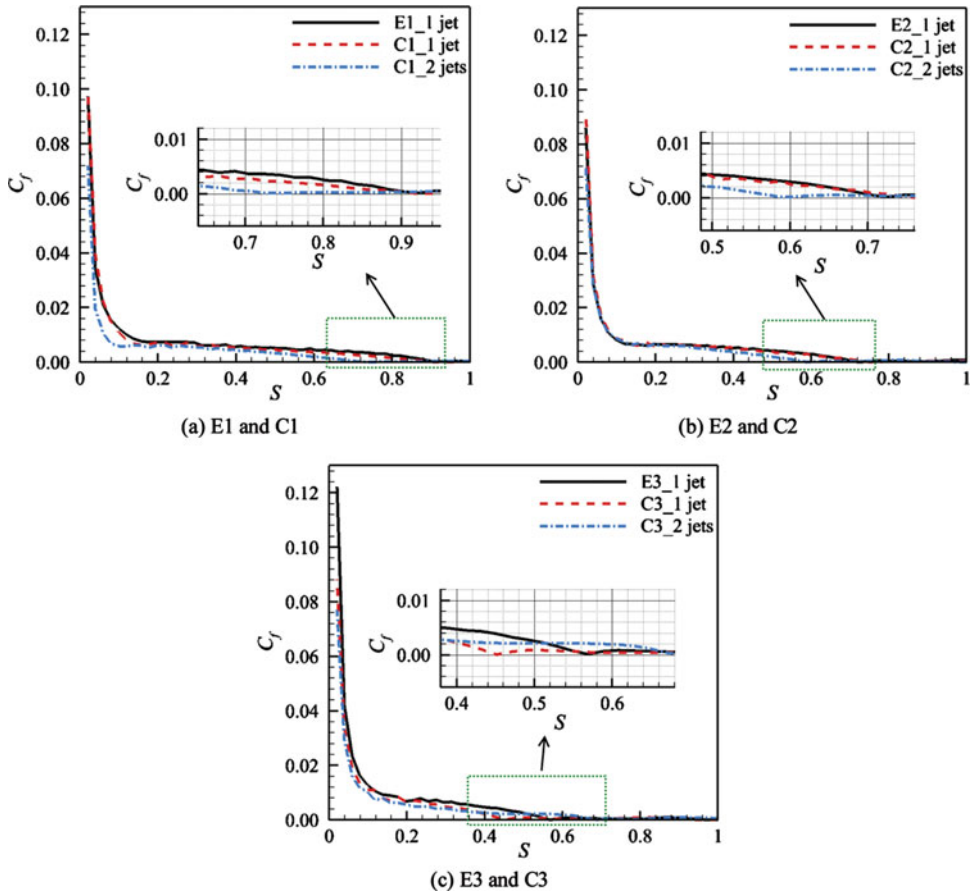

Figure 6. (Colour online) Distribution of skin friction coefficient on the Coanda surfaces, $Ma = 0.60$.

Overall, the CC cascades maintain the original aerodynamic performance or meet the flow-turning requirement of the downstream cascade with an acceptable increase in energy loss. Therefore, at this operating condition, the CC technology appears to be attractive for turbine IGVs according to our numerical simulations. The next step would be laboratory experiments.

Figure 5 shows the distribution of wall pressure coefficient (C_p) on the Coanda surface for all the cases and around the blade for case C3_1 jet and case C3_2 jets. The abscissa S in Fig. 5(a) to Fig. 5(c) indicates the dimensionless arc length of the Coanda surface, and S' in Fig. 5(d) the dimensionless arc length of the pressure surface and the suction surface (from the leading edge to the trailing edge). The wall pressure coefficient after the jet slot is lower on the circular Coanda surfaces than the elliptic ones, which means that the main flow has higher momentum at the beginning of the circular Coanda surface. The range of separation region, where the wall pressure coefficient keeps constant, increases with the increasing curvature of the Coanda surface, which shows that there is a trend of the Coanda jet detaching from the wall earlier. After adding the CFB, in Fig. 5(a) and Fig. 5(b), the curve of the wall pressure coefficient overlaps to case Coanda jet alone. In Fig. 5(c), adding the CFB reduces the range of the separation region around the trailing edge a lot, which indicates good wall attachment

https://doi.org/10.1017/aer.2017.55 Published online by Cambridge University Press

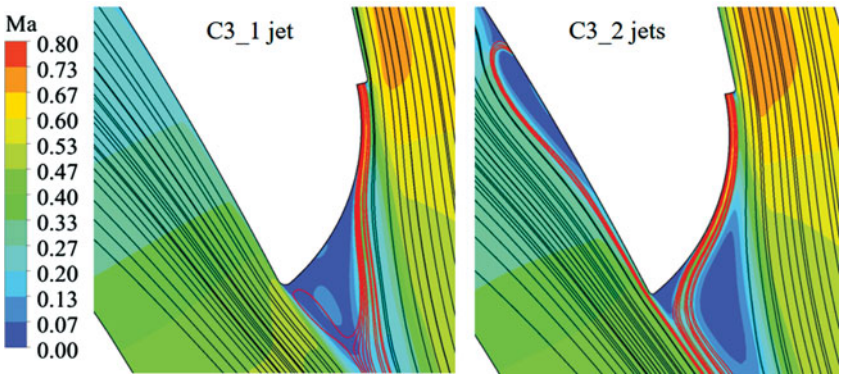

Figure 7. (Colour online) Mach number contour and streamlines around the trailing edge, $Ma = 0.60$.

of the Coanda jet. In Fig. 5(d), the pressure change on the blade leading edge is small. On the entire suction surface, the pressure decrease for the two jets case is greater and faster than the case with Coanda jet alone, which leads faster acceleration of the flow near the suction surface before the slot. There are evident pressure jumps at the blowing slots on the pressure side and also on the suction side.

Figure 6 shows the distribution of skin friction coefficient (C_f) on the Coanda surface of different circulation control cascades. The skin friction coefficient decreases as the Coanda jet flow moves downstream and becomes zero at the separation point where the jet detaches from the wall. The area that skin friction coefficient equals to zero indicates stagnation flow area. As shown in Fig. 6, the jet separation points are at $S = 0.90$, 0.70, and 0.56 on elliptic Coanda surfaces, respectively. For the circular Coanda surfaces, the location of jet separation is similar to the results on the elliptic Coanda surfaces when the counter-flow blowing is off. It indicates that the high-speed jet remains attached to the wall longer for Coanda surfaces with small curvature. Thus, the CC cascade with E1 and C1 Coanda surfaces reach the flow-turning angle of the baseline (Fig. 4). On the contrary, early Coanda jet detachment reduces the flow-turning angle, and the performance of CC cascades declines. In addition, the Coanda jet detaches from the wall at $S = 0.44$ for the C3 configuration, earlier than that on the E3 configuration ($S = 0.56$), which may suggest that the shape of the Coanda surface is more crucial as the length of the Coanda surface decreases. For C3 configuration with counter-flow blowing, the jet attachment is apparently improved, and the separation point is put off from $S = 0.45$ to $S = 0.67$. With such an improvement in wall attachment, the augmentation of the exit flow angle (0.5°) is quite limited. The reason is explained via Fig. 7.

Figure 7 shows the Mach number contour and streamlines around the trailing edge of the C3 configuration. Without counter-flow blowing (left, C3_1 jet), the Coanda jet detaches from the wall early, and a large region of low-speed fluid appears at the blade trailing edge. By adding CFB on the blade pressure side (right, C3_2 jets), the jet remains attached to the wall until close to the trailing edge, probably due to the lower wall static pressure on the suction surface and the Coanda surface than the case without CFB, as shown in Fig. 5(c) and Fig. 5(d). However, the curvature of the Coanda surface is relatively large, and the Coanda jet fails to entrain the mainstream fluid turning over such a large angle. Additionally, the axial chord length of the CC blade is only 84.10% of the original IGV, which is insufficient to vector the flow efficiently. Thus, to maintain the normal aerodynamic performance of the IGV, there

https://doi.org/10.1017/aer.2017.55 Published online by Cambridge University Press

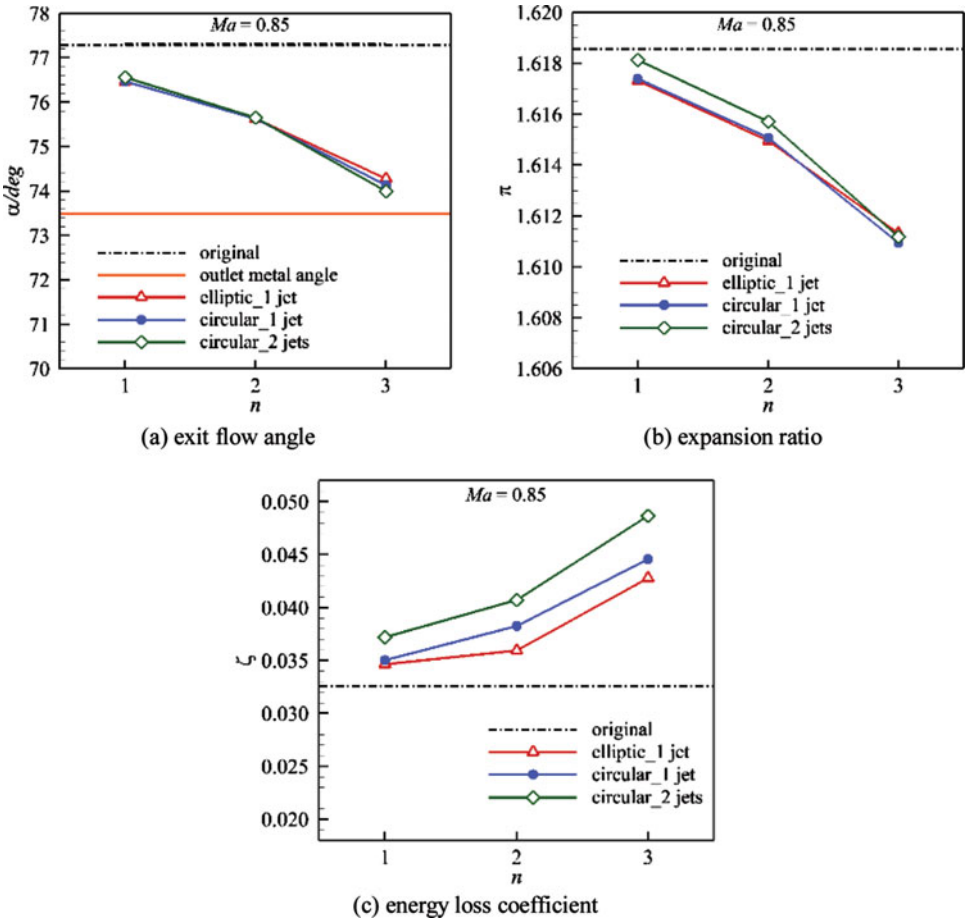

Figure 8. (Colour online) Performance parameters of the cascades, $Ma = 0.85$.

should be a limit for the minimum blade axial chord length or the maximum curvature of the Coanda surface, no matter how long the jet attaches to the wall.

4.2 Results at $Ma = 0.85$

Figure 8 shows the aerodynamic performance of the turbine cascade at $Ma = 0.85$. The general trend is basically same with the results at $Ma = 0.60$ (Fig. 4). For the elliptic and circular Coanda surfaces with the same ending points, the difference of their performance is nearly negligible. The counter-flow blowing has little influence on the exit flow angle, while the energy loss coefficient increases dramatically. For the C3 configuration, the loss is 9% higher than only Coanda jet used. Among all the circulation control cascades, case C1_2 jets obtain the largest exit flow angle (76.56°, 0.75° lower compared to the baseline) and largest expansion ratio (99.97% of the baseline). Meanwhile, the energy loss coefficient increases by 14.2%. The exit flow angles of all the CC cascades are smaller than the baseline yet larger than 73.5°, which satisfies the incidence requirement of the downstream cascade.

https://doi.org/10.1017/aer.2017.55 Published online by Cambridge University Press

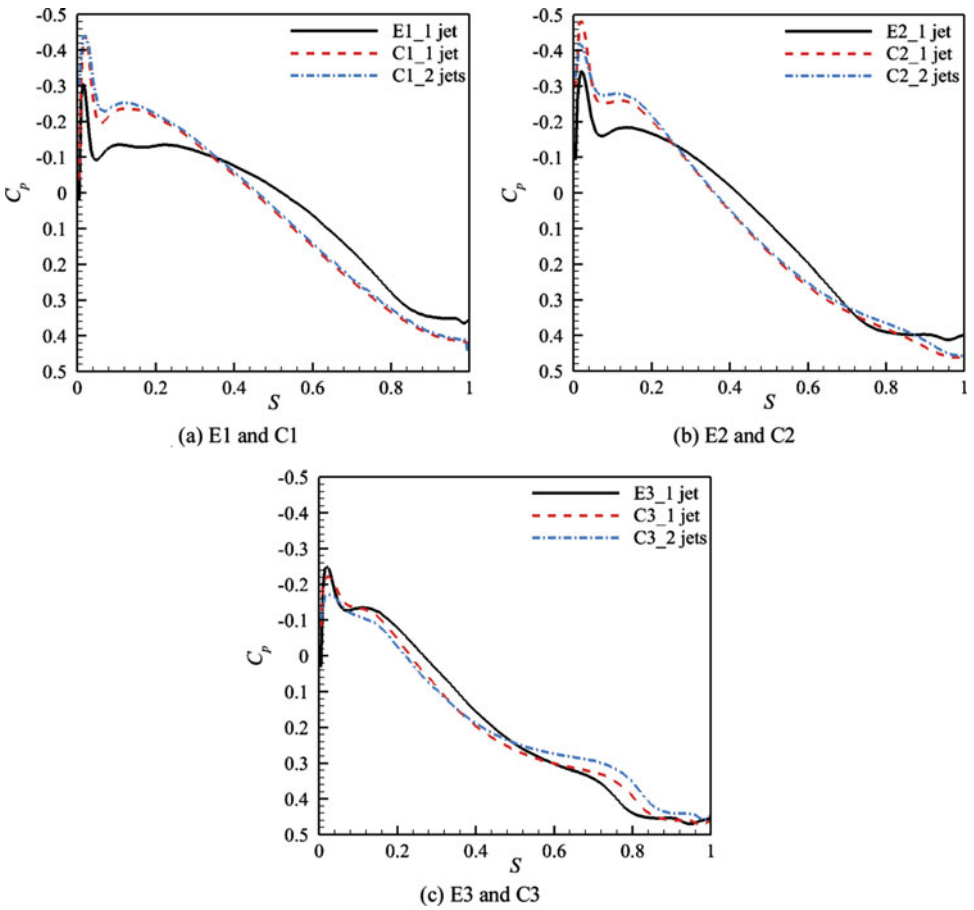

Figure 9. (Colour online) Distribution of wall pressure coefficient on the Coanda surfaces, $Ma = 0.85$.

Under the condition of exit Mach number 0.85, the counter-flow blowing cannot improve the flow-turning angle obviously but only results in the increase of the loss coefficient.

Figure 9 shows the distribution of wall pressure coefficient (C_p) on the Coanda surface. The area that the wall pressure coefficient remains constant, i.e., the stagnation area, is greatly reduced compared to the results at $Ma = 0.60$, which means the attachment of the Coanda jet is much better at $Ma = 0.85$. For the elliptic and circular Coanda surface with the same ending points, the separation region on the elliptic Coanda surfaces is mildly larger than the circular ones. Adding the CFB does not change the trend of wall pressure coefficient or the range of separation region very much.

Figure 10 shows the distribution of skin friction coefficient on the Coanda surfaces. The Coanda jet remains attached to the wall until the blade trailing edge (after $S = 0.70$) for all cases. Compared to the results at $Ma = 0.60$ (Fig. 6), the jet attachment improves significantly on the E3 and C3 Coanda surfaces. The separation points for cases E3_1 jet, C3_1 jet and C3_2 jets are at $S = 0.82$, 0.82 and 0.72, respectively. It is because at $Ma = 0.85$, the jet has relatively high momentum, which contributes to the good wall attachment results (according to the conclusion in Ref. 26) on the Coanda surface with a large curvature. Adding counter-flow

https://doi.org/10.1017/aer.2017.55 Published online by Cambridge University Press

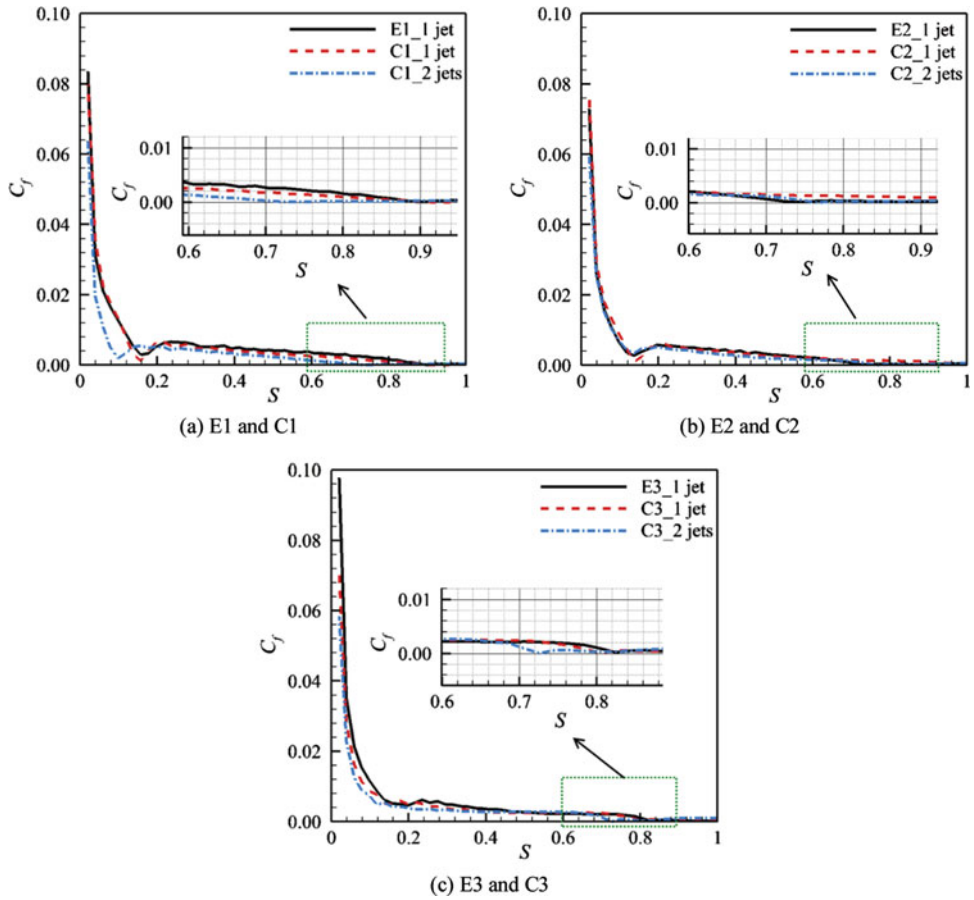

Figure 10. (Colour online) Distribution of skin friction coefficient on the Coanda surfaces, $Ma = 0.85$.

blowing (with its additional energy consumption) results in an increase in the loss coefficient but no further improvement of jet attachment or significant improvement in the flow-turning angle. Depending on the problem, it is suggested that a compromise may need to be made about whether to apply the double jet configuration.

From the above, even though with good attachment results of the Coanda jet, at $Ma = 0.85$, only the best Coanda configurations (E1 and C1) somehow work well. The performance parameters of other configurations have relatively large differences with the original cascades.

4.3 Results at $Ma = 1.10$

Figure 11 shows the aerodynamic performance of the turbine cascade at $Ma = 1.10$. Case E1_1 jet and case C1_2 jets still meet the flow-turning requirement of the downstream cascade, with exit flow angles of 73.7° and 73.6°, respectively. Case C1_2 jets also have the largest expansion ratio, which is 99.9% of the baseline, and the loss coefficient increases by 38.7%. Under supersonic exit condition, the circulation control cascades with trailing edges of small curvature still obtain better aerodynamic performance than those of large

https://doi.org/10.1017/aer.2017.55 Published online by Cambridge University Press

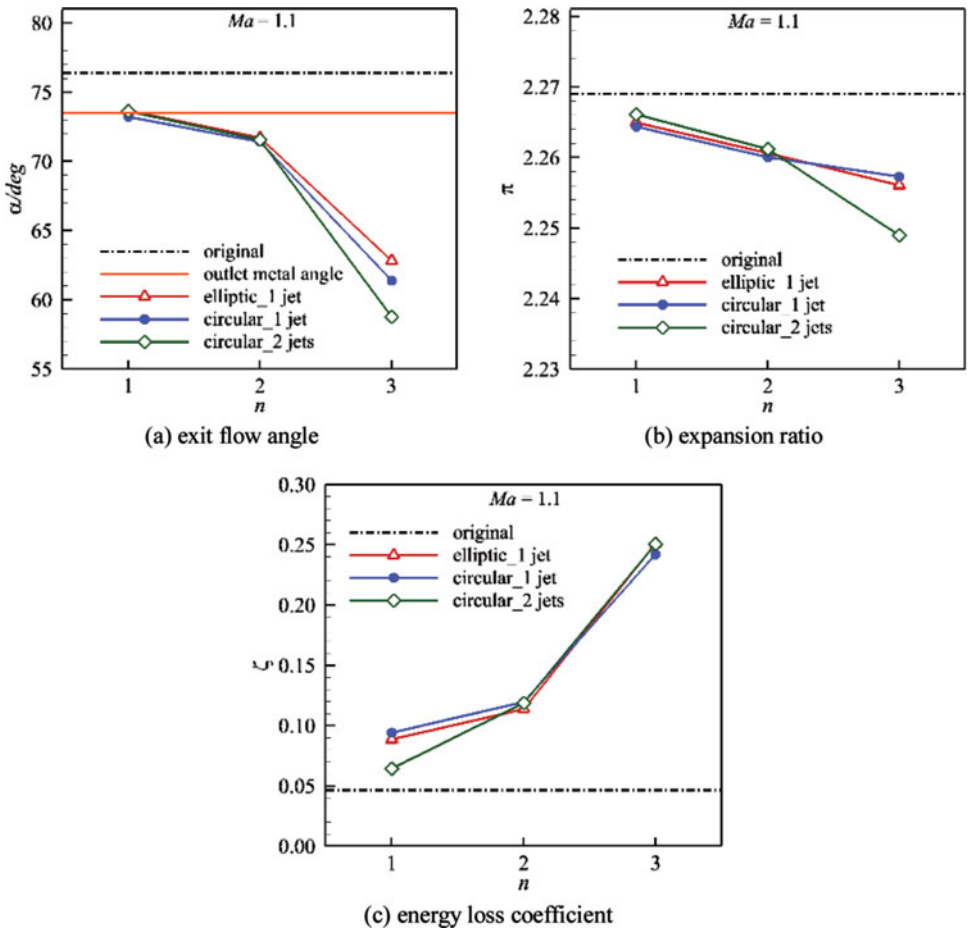

Figure 11. (Colour online) Performance parameters of the cascades, $Ma = 1.10$.

curvature. Nevertheless, compared with the high subsonic conditions, the performance differences between the CC cascades and the baseline cannot be ignored. The largest exit flow angle of the CC cascades is 2.8° lower than that of the original cascade. The reason the CC cascades performance drops sharply under supersonic exit condition can be explained via Fig. 12.

The Mach number contour and streamlines around the blade trailing edge are shown in Fig. 12. From the result of the original cascade (upper left), the main flow remains attached to the wall along the entire suction surface. Due to supersonic flow at the exit, a shock wave forms at the very end of the suction surface. For the configurations of E1_1 jet (upper middle), C1_1 jet (upper right), and C1_2 jets (lower left), a premature shock wave appears on the Coanda surface near the jet slot, with a local Mach number of about 1.50 ahead of the shock. For the baseline, the Mach number ahead of the shock is around 1.35. If *Ma* is much greater than 1.35, shock-induced flow separation is almost unavoidable. The Coanda shapes have too much aft camber for these Mach numbers. Shock wave/ boundary-layer interactions cause jet detachment and deflection of the mainstream. As a result, the flow-

https://doi.org/10.1017/aer.2017.55 Published online by Cambridge University Press

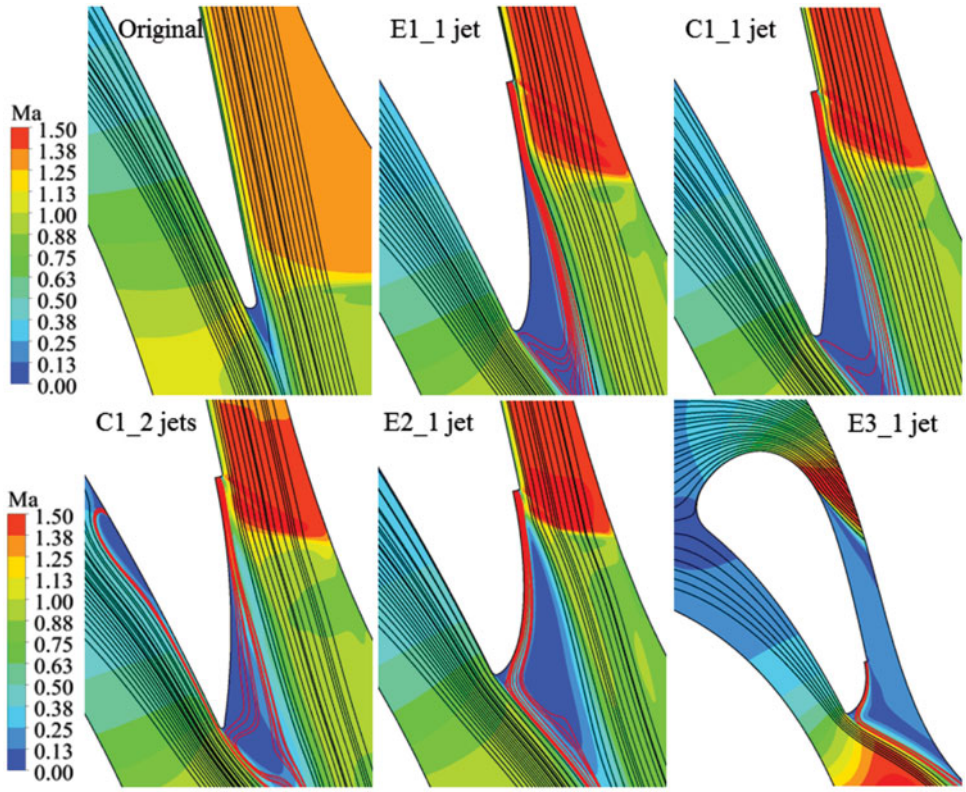

Figure 12. (Colour online) Mach number contour and streamlines around the trailing edge, $Ma = 1.10$.

turning angle decreases. With only the Coanda jet applied, the shock wave occurs slightly later on the E1 Coanda surface than on the C1 Coanda surface. With counter-flow blowing applied, the location of the shock wave keeps unchanging, while the Coanda jet remains attached to the wall a little longer. The Mach number contours and streamlines of cases E2_1 jet (lower middle) and E3_1 jet (lower right) are also shown in Fig. 12. For both cases, the Coanda jet maintains good attachment because of the Coanda effect. However, a shock wave appears near the jet slot on the Coanda surface for case E2_1 jet and at the front part of the suction surface for case E3_1 jet. The shock wave leads the flow separation of the mainstream, and the flow condition deteriorates severely, which can explain the large energy loss in CC cascades. The Coanda jet cannot entrain the main flow due to the stagnation area between them.

Figure 13 shows the distribution of wall pressure coefficient (C_p) on the Coanda surface. The trend of wall pressure coefficient at this condition is evidently different from the results at $Ma = 0.60$ and $Ma = 0.85$. Because of the shock wave, there is only a short range where the wall pressure coefficient increases quickly on the Coanda surfaces, and then it increases at a small slope or fluctuates, which means that the Coanda jet detaches from the wall early. Adding the CFB does not change the trend of wall pressure coefficient very much except for C3 configuration, where the wall pressure coefficient increases faster than the only Coanda jet case from $S = 0.36$.

https://doi.org/10.1017/aer.2017.55 Published online by Cambridge University Press

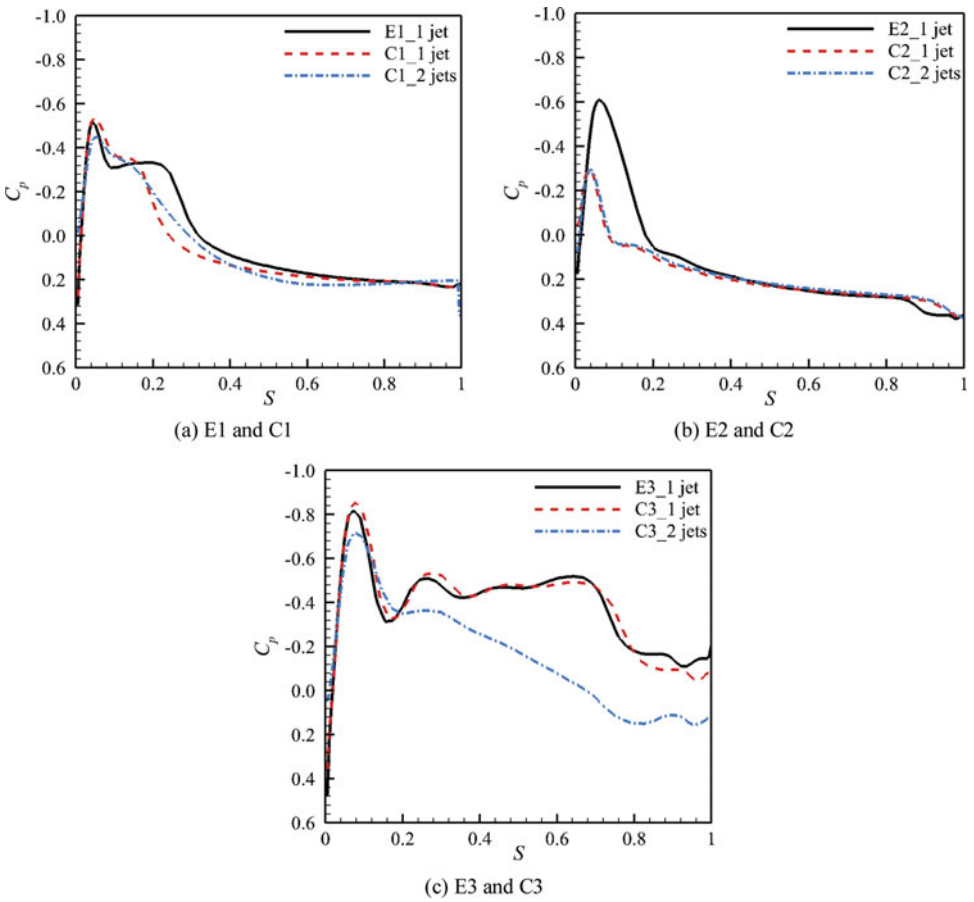

Figure 13. (Colour online) Distribution of wall pressure coefficient on the Coanda surfaces, $Ma = 1.10$.

Figure 14 shows the distribution of skin friction coefficient on the Coanda surfaces at $Ma = 1.10$, which is evidently different with the results at high subsonic conditions. Because of the shock wave, the Coanda jet detaches from the wall around $S = 0.43$ for case E1_1 jet. The skin friction coefficient of the case C1_1 jet never falls to zero but from Fig. 12, the jet detaches from the wall very early. Adding counter-flow blowing moves the jet detachment point even forward to around $S = 0.36$. In Fig. 14(b) and Fig. 14(c), the skin friction coefficient falls down to near zero and then becomes positive before being zero again. It may indicate the unsteady condition of the Coanda jet, i.e., at a critical point of separation, or some reverse flow area. The streamlines near the Coanda surface indicate that the Coanda jet is well attached to the wall for the E2 and E3 configurations, as well as for cases C2 and C3, which are not shown in Fig. 12. The jets remain attached to the wall until the end of the Coanda surface for E2 and C2 and separate at around $S = 0.80$ for E3 and C3, which indicates that the shock wave has no obvious influence on the wall attachment of the Coanda jet for these cases. However, having good jet attachment is of no help here for entraining the main flow. The shape of the Coanda surface must be designed carefully to delay or even eliminate the shock wave when the exit flow is supersonic. Nevertheless, it is still hard to say that

https://doi.org/10.1017/aer.2017.55 Published online by Cambridge University Press

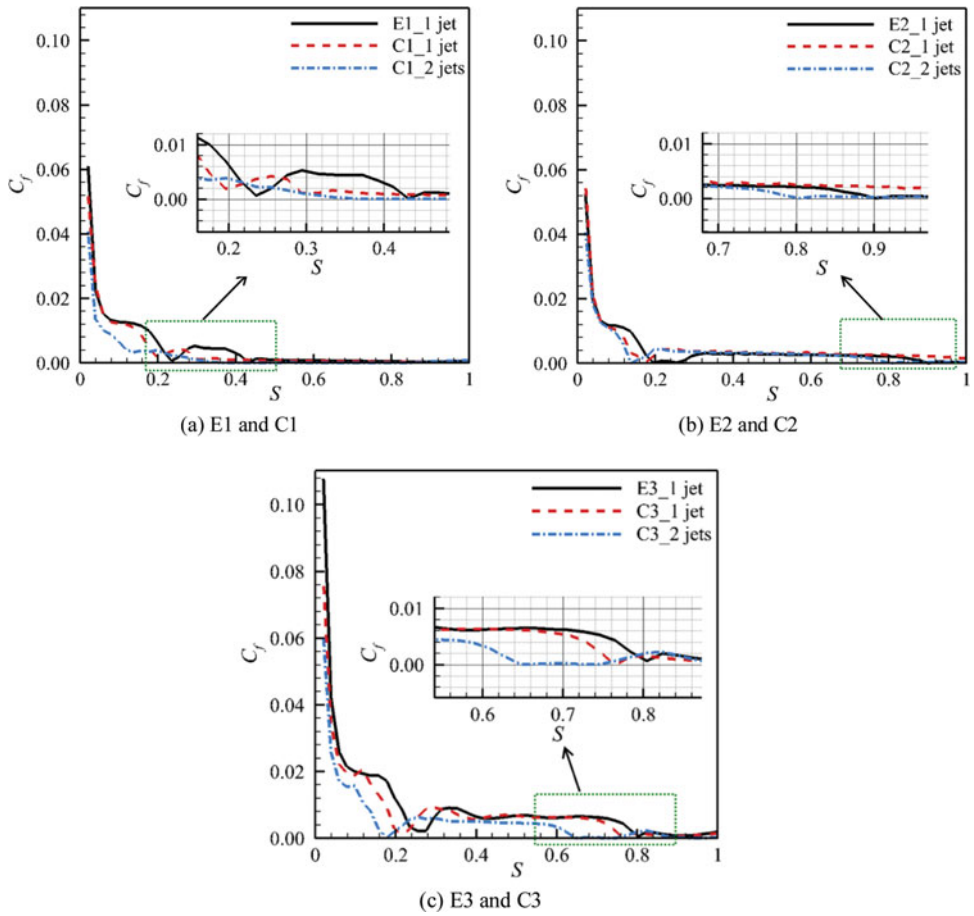

Figure 14. (Colour online) Distribution of skin friction coefficient on the Coanda surfaces, $Ma = 1.10$.

the CC cascades will definitely out-perform the baseline, which needs some experimental validation.

5.0 CONCLUSIONS

The application of the Coanda effect on a circulation-control turbine cascade was studied via numerical simulation under high subsonic and supersonic conditions. The effects of differently shaped Coanda surfaces, a Coanda jet, and counter-flow blowing on the aerodynamic performance of turbine cascades were investigated. The following conclusions can be drawn.

With the exit Mach numbers of 0.60 and 0.85, by adding a total jet mass flow of around 3% of the main mass flow, the circulation control cascade regains the aerodynamic performance of the original cascade with a 13.52% reduction in axial chord length, which demonstrates that the circulation control technology has the potential for weight-reduction in turbine cascades. The circular and elliptic Coanda surfaces with the same starting and ending points obtain similar aerodynamic performances. When the curvature is large and the area

https://doi.org/10.1017/aer.2017.55 Published online by Cambridge University Press

of Coanda surface becomes small, the performance of circulation control cascade is more sensitive to the shape of the Coanda surface. Increasing the Coanda surface curvature leads to early detachment of the Coanda jet from the wall, resulting in a drop of the aerodynamic performance in circulation control cascades.

The lower wall static pressure on the suction surface and the Coanda surface in the case with CFB encourages the Coanda jet to stay attaching to the Coanda surfaces with a large curvature, which results in slightly larger exit flow angles and expansion ratios. Because the energy consumption of the two jets is also taken into account, the energy loss increases correspondingly. For specific conditions, a compromise may need to be made about whether to add counter-flow blowing. Further studies are necessary to enhance the efficiency of jet entrainment on Coanda surfaces with large curvature.

The overall aerodynamic performance of the circulation control cascades at $Ma = 1.10$ is poor and has a large difference with the baseline. A premature shock wave can appear near the jet slot on the Coanda surface in circulation control cascades. The shock wave has no obvious effect on the wall attachment of the Coanda jet but causes the deterioration of the main flow condition. It becomes more difficult for the modified cascades to match the flow-turning angle of the baseline. Thus, a more reliable shape of the Coanda surface needs to be found to delay or even to eliminate the shock wave.

ACKNOWLEDGEMENTS

The work was supported by the National Natural Science Foundation of China (grant number 50876023); and the Specialised Research Fund for the Doctoral Program of Higher Education (grant number 200802130017). The authors also acknowledge that AIAA has granted permission for reuse of the picture materials from the work of Novak et al[29].

REFERENCES

1. ENGLAR, R.J. Circulation control pneumatic aerodynamics-blown force and moment augmentation and modification; past, present and future, AIAA Fluids Conference and Exhibit, 19–22 June 2000, Denver, CO, US, AIAA Paper 2000-2541.
2. KWEDER, J., PANTHER, C.C. and SMITH, J.E. Applications of circulation control, yesterday and today, *Int J Engineering*, 2010, **4**, (5), pp 411-429.
3. JONES, G.S., VIKEN, S.A., WASHBURN, A.E., JENKINS, L.N. and CAGLE, C.M. An active flow circulation controlled flap concept for general aviation aircraft applications, Proceedings of 1st AIAA Flow Control Conference, 24–26 June 2002, St. Louis, Minnesota, US, AIAA Paper 2002-3157.
4. COOK, M.V., BUONANNO, A. and ERBSLOH, S.D. A circulation control actuator for flapless flight control, *Aeronaut J*, August 2008, **112**, (1134), pp 483-489.
5. LIU, Y. and SANKAR, L.N. Computational evaluation of controlling flap edge vortex and tip vortex effects with circulation control technique, Proceedings of 45th AIAA Aerospace Sciences Meeting and Exhibit, 8–11 January 2007, Reno, Nevada, US, AIAA Paper 2007-473.
6. KANISTRAS, K., RUTHERFORD, M.J., VITZILAIOS, N. and VALAVANIS, K.P. Experimental study of circulation control wings at low Reynolds numbers, Proceedings of 32nd AIAA Applied Aerodynamics Conference, 16–20 June 2014, Atlanta, Georgia, US, AIAA Paper 2014-2307.
7. ABRAMSON, J. and ROGERS, E.O. High- speed characteristics of circulation control airfoils, Proceedings of 21st AIAA Aerospace Sciences Meeting, 10–13 January 1983, Reno, Nevada, US, AIAA Paper 1983-0265.

https://doi.org/10.1017/aer.2017.55 Published online by Cambridge University Press

8. SCHLECHT, R. and ANDERS, S. Parametric evaluation of thin, transonic circulation control airfoils, Proceedings of 45th AIAA Aerospace Sciences Meeting and Exhibit, 8–11 January 2007, Reno, Nevada, US, AIAA Paper 2007-272.
9. ZEUNE, C.H. An overview of the Air Force's speed agile concept demonstration program, Proceedings of 51st AIAA Aerospace Sciences Meeting including the New Horizons Forum and Aerospace Exposition, 7–10 January 2013, Grapevine (Dallas/Ft. Worth Region), Texas, US, AIAA Paper 2013-1097.
10. WICK, A.T., HOOKER, J.R., BARBERIE, F.J. and ZEUNE, C.H. Powered lift CFD predictions of a transonic cruising STOL military transport, Proceedings of 51st AIAA Aerospace Sciences Meeting including the New Horizons Forum and Aerospace Exposition, 7–10 January 2013, Grapevine (Dallas/Ft. Worth Region), Texas, US, AIAA Paper 2013-1098.
11. BARBERIE, F.J., HOOKER, J.R. and ZEUNE, C.H. Low speed powered lift testing of a transonic cruise efficient STOL military transport, *Proceedings of 51st AIAA Aerospace Sciences Meeting including the New Horizons Forum and Aerospace Exposition*, 07–10 January 2013, Grapevine (Dallas/Ft. Worth Region), Texas, US, AIAA Paper 2013-1099.
12. HOOKER, J.R., WICK, A.T., ZEUNE, C.H., JONES, G. and MILHOLEN, W. Design and transonic wind tunnel testing of a cruise efficient STOL military transport, Proceedings of 51st AIAA Aerospace Sciences Meeting including the New Horizons Forum and Aerospace Exposition, 7–10 January 2013, Grapevine (Dallas/Ft. Worth Region), Texas, US, AIAA Paper 2013-1100.
13. JONES, G.S., LIN, J.C., ALLAN, B.G., MILHOLEN, W.E., RUMSEY, C.L. and SWANSON, R.C. Overview of CFD validation experiments for circulation control applications at NASA, RAES-566-8A1, International Powered Lift Conference, July 2008, London, UK.
14. MILHOLEN, W.E., JONES, G.S., CHAN, D.T. and GOODLIFF, S.L. Enhancements to the FAST-MAC circulation control model and recent high-Reynolds number testing in the national transonic facility, Proceedings of 31st AIAA Applied Aerodynamics Conference, 24–27 June 2013, San Diego, CA, US, AIAA Paper 2013-2794.
15. CHAN, D.T., MILHOLEN, W.E., JONES, G.S. and GOODLIFF, S.L. Thrust removal methodology for the FAST-MAC circulation control model tested in the national transonic facility, 32nd AIAA Applied Aerodynamics Conference, AIAA Paper 2014-2402.
16. FORSTER, M. and STEIJL, R. Numerical simulation of transonic circulation control, 53rd AIAA Aerospace Sciences Meeting, 5–9 January 2015, Kissimmee, Florida, US, AIAA Paper 2015-1709.
17. FORSTER, M., BIAVA, M. and STEIJL, R. Multipoint optimisation of Coanda surfaces for transonic circulation control using the adjoint method, *8th AIAA Flow Control Conference, AIAA Aviation and Aeronautics Forum and Exposition,* 13–17 June 2016, Washington, DC, US, AIAA Paper 2016-3773.
18. DISKIN, B., THOMAS, J.L., RUMSEY, C.L. and SCHWOPPE, A. Grid-convergence of Reynolds-averaged Navier–Stokes solutions for benchmarck flows in two dimensions, *AIAA J*, 2016, **54**, (9), pp 2563-2588.
19. KRUGER, R.A., MARSH, H. and HORLOCK, J.H. The performance of a cascade fitted with blown flaps, CP-526, Aeronautical Research Council, Great Britain, 1961.
20. LORD, W.K., MACMARTIN, D.G. and TILLMAN, G. Flow control opportunities in gas turbine engines, AIAA Fluids Conference and Exhibit, 19–22 June 2000, Denver, CO, US, AIAA Paper 2000-2234.
21. HILL, H.E., NG, W.F., VLACHOS, P.P., GUILLOT, S.A. and CAR, D. 2D parametric study using CFD of a circulation control inlet guide vane, Proceedings of ASME Turbo Expo Power for Land, Sea and Air, 14–17 May 2007, Montreal, Canada, GT2007-28058.
22. GUENDOGDU, Y., VORREITER, A. and SEUME, J.R. Design of a low solidity flow-controlled station with Coanda surface in a high speed compressor, Proceedings of ASME Turbo Expo Power for Land, Sea and Air, 9–13 June 2008, Berlin, Germany, GT2008-51180.
23. FISCHER, S., SAATHOFF, H. and RADESPIEL, R. Numerical and experimental investigation on a low-speed compressor cascade with circulation control, Proceedings of ASME Turbo Expo Power for Land, Sea and Air, 9–13 June 2008, Berlin, Germany, GT2008-50302.
24. FISCHER, S., MULLER, L., SAATHOFF, H. and KOZULOVIC, D. Three-dimensional flow through a compressor cascade with circulation control, Proceedings of ASME Turbo Expo, 11–15 June 2012, Copenhagen, Denmark, GT2012-68593.

https://doi.org/10.1017/aer.2017.55 Published online by Cambridge University Press

25. HARFF, M.R., WOLFF, J.M. and COPENHAVER, W.W. A CFD investigation of IGV flow vectoring by counter flow, Proceedings of ASME Turbo Expo Power for Land, Sea and Air, 14–17 June 2004, Vienna, Austria, GT2004-53941.
26. SONG, Y., LI, Y., CHEN, H. and CHEN, F. Two-dimensional simulation of circulation control turbine cascade, *Proceedings of the Institution of Mech Engineers, Part G: J Aerospace Engineering*, 2011, **225**, (7), pp 761-767.
27. ANSYS CFX 12.0, ANSYS, Inc., www.ansys.com.
28. ANSYS ICEM 12.0, ANSYS, Inc., www.ansys.com.
29. NOVAK, C.J., CORNELIUS, K.C. and ROADS, R.K. Experimental investigations of the circular wall jet on a circulation control airfoil, Proceedings of 25th AIAA Aerospace Sciences Meeting, 12–25 January 1987, Reno, Nevada, US, AIAA Paper 1987-0155.

https://doi.org/10.1017/aer.2017.55 Published online by Cambridge University Press